Inorg. Chem. **2008**, *47*, 10753−10757

$La_8Br_7Ni_4$: Ribbons of Ni Hexagons in Condensed La_6 Trigonal Prisms

Chong Zheng,*,† Hansjürgen Mattausch,‡ Constantin Hoch,‡ and Arndt Simon*,‡

Department of Chemistry and Biochemistry, Northern Illinois University, DeKalb, Illinois 60115, and Max-Planck-Institut für Festkörperforschung, Heisenbergstrasse 1, D-70569 Stuttgart, Germany

Received July 2, 2008

A ternary lanthanum bromide $La_8Br_7Ni_4$ was synthesized from La, $LaBr_3$, and Ni under an Ar atmosphere at 830 °C. It crystallizes in space group *C*2/*m* (No. 12) with lattice constants $a = 29.528(4)$ Å, $b = 4.0249(6)$, $c = 8.708(1)$ Å, and $\beta = 94.515(2)°$. The structure features condensed Ni-centered La_6 trigonal prisms. The Ni atoms are bonded to each other to form ribbons of Ni hexagons. Band structure, bonding, and physical properties of the compound have been investigated.

Introduction

Reduced rare earth (RE) metal halide chemistry is rich in its structural variations. Yet in most cases, the structures are based on RE_6 octahedra or trigonal prisms which are centered by a great number of main group or transition metal atoms ranging from hydrogen to gold.[1−13] These polyhedra can be isolated or condensed by sharing their corners, edges, or faces. In this class, not many Ni-containing compounds have been reported. To our knowledge, Ln_2INi_2 (Ln = La, Pr) so far were the only members of the family containing connected Ni in a condensed cluster system.[14,15] Still another Ni-containing reduced rare earth metal halide, Pr_4I_5Ni, features isolated Ni atoms inside condensed Pr octahedra.[15] In this contribution, we report the synthesis, structure determination, electronic structure analysis and physical property measurement of a new compound, $La_8Br_7Ni_4$, for which both La−La and Ni−Ni bonding is significant.

Experimental Section

Synthesis. La metal (sublimed, 99.99%; Alfa-Aesar, small pieces), $LaBr_3$, and Ni (powder, 99.99%; Aldrich) were used as starting materials. $LaBr_3$ was prepared by the reaction of La_2O_3 with concentrated HBr and NH_4Br;[16] the product was then dried under a dynamic vacuum and purified twice by sublimation in a Ta container before use. Due to the air and moisture sensitivity of the reactants and the product, all handling was carried out under an Ar atmosphere either in a glovebox or through the standard Schlenk technique.

The stoichiometric mixture (ca. 1.0 g) of the starting materials was arc-sealed in a Ta tube under an Ar atmosphere. The Ta tube was then sealed inside a silica glass ampoule under a vacuum of ca. 10^{-2} mbar. The reaction was carried out at 830 °C for 19 days. After the reaction, the ampoule was quenched in water and then opened under an Ar atmosphere. Many needle-like single crystals with dark metallic reflectance were observed in the product. The yield, estimated from a Guinier powder X-ray measurement, was nearly 100%. No other phases could be detected from the powder X-ray pattern and from the energy dispersive X-ray (EDX) analyses. EDX analyses of these single crystals, using a TESCAN scanning electron microscope equipped with an Oxford EDX detector,

* Authors to whom correspondence should be addressed. E-mail: czheng@niu.edu (C.Z.), a.simon@fkf.mpg.de (A.S.).
† Northern Illinois University.
‡ Max-Planck-Institut für Festkörperforschung.

(1) Simon, A.; Mattausch, Hj.; Miller, G. J.; Bauhofer, W.; Kremer, R. K. Metal-Rich Halides. In *Handbook on the Physics and Chemistry of Rare Earths*; Elsevier Science Publishers: Amsterdam, 1991; Vol. *15*, p 191.
(2) Mattausch, Hj.; Simon, A. *Angew. Chem., Int. Ed.* **1998**, *37*, 499. Mattausch, Hj.; Simon, A. *Angew. Chem.* **1998**, *110*, 498.
(3) Mattausch, Hj.; Oeckler, O.; Simon, A. *Inorg. Chim. Acta* **1999**, *289*, 174.
(4) Warkentin, E.; Simon, A. *Rev. Chim. Miner.* **1983**, *20*, 488.
(5) Nagaki, D.; Simon, A.; Borrmann, H. *J. Less-Common Metals* **1989**, *156*, 193.
(6) Dorhout, P. K.; Payne, M. W.; Corbett, J. D. *Inorg. Chem.* **1991**, *30*, 4960.
(7) Llusar, R.; Corbett, J. D. *Inorg. Chem.* **1994**, *33*, 849.
(8) Hughbanks, T.; Rosenthal, G.; Corbett, J. D. *J. Am. Chem. Soc.* **1986**, *108*, 8289.
(9) Hughbanks, T.; Corbett, J. D. *Inorg. Chem.* **1988**, *27*, 2022.
(10) Hughbanks, T.; Corbett, J. D. *Inorg. Chem.* **1989**, *28*, 631.
(11) Meyer, G.; Wickleder, M. S. Simple and Complex Halides. In *Handbook on the Physics and Chemistry of Rare Earths*; Elsevier Science Publishers: Amsterdam, 2000; Chapter 177, Vol. *28*, pp 53.
(12) Corbett, J. D. *J. Chem. Soc., Dalton Trans.* **1996**, 575.
(13) Simon, A.; Mattausch, Hj.; Ryazanov, M.; Kremer, R. K. *Z. Anorg. Allg. Chem.* **2006**, *632*, 919.
(14) Hong, S.-T.; Martin, J. D.; Corbett, J. D. *Inorg. Chem.* **1998**, *37*, 3385.
(15) Park, Y.; Martin, J. D.; Corbett, J. D. *J. Solid State Chem.* **1997**, *129*, 277.
(16) Meyer, G.; Ax, P. *Mater. Res. Bull.* **1982**, *17*, 1447.

10.1021/ic801227e CCC: $40.75
Published on Web 10/24/2008

Table 1. Crystal Data and Structure Refinement for $La_8Br_7Ni_4$

fw	1905.49
temperature	293(2) K
wavelength	0.71073 Å
cryst syst	monoclinic
space group	*C*2/*m*
unit cell dimensions	$a = 29.528(4)$ Å
	$b = 4.0249(6)$ Å
	$c = 8.708(1)$ Å
	$\beta = 94.515(2)°$
vol/*Z*	1031.7(3) Å^3/2
density (calculated)	6.134 Mg/m^3
abs coeff	33.243 mm^{-1}
index ranges	$-34 \le h \le 34$, $-4 \le k \le 4$, $-10 \le l \le 10$
reflns collected	3677
independent reflns	1049 [R(int) = 0.0281]
abs correction	semiempirical from equivalents[33]
refinement method	full-matrix least-squares on F^2
data/restraints/params	1049/0/59
goodness-of-fit on F^2	1.262
final R indices [$I > 2\sigma(I)$][a]	$R_1 = 0.0310$, $wR_2 = 0.0975$
R indices (all data)	$R_1 = 0.0339$, $wR_2 = 0.0990$
largest diff. peak and hole	2.077 and −1.897 e Å^{-3}

[a] $R_1 = \sum||F_o| - |F_c||/\sum|F_o|$. $wR_2 = [\sum[w(F_o^2 - F_c^2)^2]/\sum[w(F_o^2)^2]]^{1/2}$.

confirmed the presence of the component elements in the atomic percentage ratio of 39.9(3):42(2):19(2) (La/Br/Ni) averaged over three spectra.

Structure Determination. The reaction product was ground to fine powder under an Ar atmosphere and sealed in a glass capillary for phase identification by a modified Guinier technique[17] (Cu Kα_1: $\lambda = 1.54056$ Å; internal standard Si with $a = 5.43035$ Å; Fujifilm BAS-5000 image plate system). Single crystals were transferred to glass capillaries under Na-dried paraffin oil and sealed under an Ar atmosphere. They were first examined by the precession technique before being characterized on a Bruker SMART CCD diffractometer. Absorption and polarization effect corrections were applied through the program SADABS.[18] The structure was solved with direct methods using the SIR97 program.[19] Full matrix least-squares refinement on F^2 was carried out using the SHELXTL package.[18]

$La_8Br_7Ni_4$ crystallizes in the monoclinic space group *C*2/*m* (No. 12) with lattice $a = 29.528(4)$ Å, $b = 4.0249(6)$, $c = 8.708(1)$ Å, and $\beta = 94.515(2)°$. The R_1 and wR_2 factors converged to 0.0310 and 0.0975, respectively, during the refinement. The crystallographic information including the fractional coordinates and selected bond lengths of the compound is listed in Tables 1−3.

Computational Study. The density of states (DOS) and crystal orbital overlap populations (COOP) were both computed using the tight-binding extended Hückel method (EH).[20,21] A total of 128 k points in the irreducible wedge of the Brillouin zone were used in the EH computations. The EH parameters in the computation are listed in Table 4.

Physical Property Measurements. For conductivity measurement, the polycrystalline samples were pressed into pellets of 5 mm in diameter and ca. 2 mm in thickness. The conventional four-contact method[22] was used. Susceptibility measurements were carried out on a Quantum Design PPMS 6000 magnetometer, using sample quantities of ca. 50 mg.

Table 2. Atomic Coordinates ($\times 10^4$) and Equivalent Isotropic Displacement Parameters (Å$^2 \times 10^3$) for $La_8Br_7Ni_4$[a]

atom	Wyckoff Position	x	y	z	U(eq)
La(1)	4*i*	126(1)	0	8066(1)	16(1)
La(2)	4*i*	1275(1)	5000	−645(1)	17(1)
La(3)	4*i*	2104(1)	0	2261(1)	17(1)
La(4)	4*i*	984(1)	5000	3533(1)	17(1)
Br(1)	4*i*	2126(1)	0	−1331(2)	19(1)
Br(2)	4*i*	1037(1)	0	6450(1)	19(1)
Br(3)	2*d*	0	5000	5000	20(1)
Br(4)	4*i*	1989(1)	5000	4902(2)	19(1)
Ni(1)	4*i*	988(1)	0	1327(2)	19(1)
Ni(2)	4*i*	411(1)	5000	535(2)	19(1)

[a] U(eq) is defined as one third of the trace of the orthogonalized U_{ij} tensor.

Table 3. Selected Interatomic Distances [Å] in $La_8Br_7Ni_4$

Bonds (multiplicity)	Distances
La(1)−La(1)	3.505(2)
La(1)−La(2) (2×)	4.030(1)
La(1)−La(4) (2×)	4.001(1)
La(2)−La(2)	4.0249(6)
La(2)−La(3) (2×)	3.933(1)
La(2)−La(4)	3.803(1)
La(3)−La(3)	4.0249(6)
La(3)−La(4) (2×)	4.098(1)
La(4)−La(4)	4.0249(6)
La(1)−Ni(1) (2×)	3.371(2)
La(1)−Ni(2) (2×)	2.889(2)
La(1)−Ni(2) (2×)	3.016(1)
La(2)−Ni(1) (2×)	2.819(1)
La(2)−Ni(2)	2.826(2)
La(3)−Ni(1)	3.333(2)
La(4)−Ni(1) (2×)	2.783(1)
La(4)−Ni(2)	2.998(2)
La(1)−Br(2)	3.134(2)
La(1)−Br(3) (2×)	3.3405(7)
La(2)−Br(1) (2×)	3.309(1)
La(2)−Br(2) (2×)	3.266(1)
La(3)−Br(1)	3.133(2)
La(3)−Br(1) (2×)	3.188(1)
La(3)−Br(4) (2×)	3.095(1)
La(3)−Br(4) (2×)	3.498(2)
La(4)−Br(2) (3×)	3.235(1)
La(4)−Br(3)	3.2659(9)
La(4)−Br(4)	3.107(2)
Ni(1)−Ni(2) (2×)	2.692(2)
Ni(2)−Ni(2)	2.529(4)

Table 4. Extended Hückel Parameters

	orbital	H_{ii} (eV)	ζ_1[a]	ζ_2	c_1[a]	c_2
La	6s	−7.67	2.14			
	6p	−5.01	2.08			
	5d	−8.21	3.78	1.381	0.7765	0.4586
Br	4s	−22.07	2.588			
	4p	−13.1	2.131			
Ni	4s	−9.17	1.825			
	4p	−5.15	1.125			
	3d	−13.49	5.75	2.000	0.5683	0.6292

[a] Exponents and coefficients in a double-ζ expansion of the d orbital.

Results and Discussion

Crystal Structure. The projection of the crystal structure of $La_8Br_7Ni_4$ along [010] is shown in Figure 1. It features condensed La_6 trigonal prisms. They share side rectangular faces to form a chain, and two such chains are further joined together to form a double column in the *b* direction. There

(17) Simon, A. *J. Appl. Crystallogr.* **1970**, *3*, 11.
(18) Sheldrick, G. M. *SHELXTL*, version 6.10; Bruker Analytical Instruments Inc.: Madison, WI, 2000.
(19) Altomare, A.; Burla, M. C.; Camalli, M.; Cascarano, G. L.; Giacovazzo, C.; Guagliardi, A.; Moliterni, A. G. G.; Polidori, G.; Spagna, R. *J. Appl. Crystallogr.* **1999**, *32*, 115.
(20) Hoffmann, R. *J. Chem. Phys.* **1963**, *39*, 1397.
(21) Whangbo, M. H.; Hoffmann, R.; Woodward, R. B. *Proc. R. Soc. London* **1979**, *A366*, 23.
(22) van der Pauw, L. J. *Philips Res. Rev.* **1958**, *13*, 1.

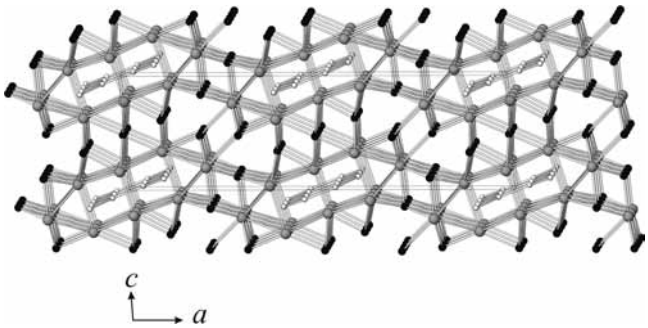

Figure 1. Projection of the $La_8Br_7Ni_4$ crystal structure along [010]. The gray spheres are La, black are Br, and white are Ni.

are two such columns per unit cell. The side rectangular faces of these columns are capped by a second type of La atom (La3), and the top and bottom triangular faces by Br atoms. Similar types of condensed trigonal prisms have been observed in a number of other reduced rare earth metal halides and related compounds. Nearly identical columns occur in $Pr_8Cl_7B_7$[23] and Ce_3Br_3BC,[24] layers in $La_3I_2Al_2$,[25] and single chains in $Bi_{12}I_3Ni_4$[26] and $Bi_{7-\delta}Br_5Ni_2$ ($\delta \approx 0.11$).[27] Ni atoms in $La_8Br_7Ni_4$ occupy positions inside these La_6 trigonal prisms. Ni(1) nearly centers the basis of a tetragonal pyramid of La atoms, and Ni(2) is significantly shifted from the center of the La_6 trigonal prism toward its Ni(2) neighbor. The average Ni−La distance around Ni(1) is by 0.1 Å larger than that around Ni(2), in accordance with the difference in Ni−La coordination numbers, 7 and 6, respectively. The 7-coordination environment for Ni is similar to that of Al in $La_3I_2Al_2$.[25] The Ni atoms form hexagons propagating in the *b* direction similar to a polyacene ribbon (Figure 2). This type of ribbon has been observed for Al in $La_3I_2Al_2$,[25] and for B in Ta_3B_4, whose electronic structure has been investigated in detail by Minyaev and Hoffmann.[28] The Ni−Ni distances are 2.529 Å for the shared edges of the hexagons (Ni2−Ni2) and 2.692 Å for the others (Ni1−Ni2). This difference in bond length ($\Delta d_{Ni-Ni} = 0.163$ Å) is larger than in the polyacene-like Al ribbon in the structure of $La_3I_2Al_2$ ($\Delta d_{Al-Al} = 0.065$ Å). The shorter inner bond can therefore be formally assigned to a double bond (see the next section). Similarly connected transition metal networks have been found in other reduced rare earth metal halides such as Gd_2IFe_2,[29] where the graphene-like Fe network is puckered as it is also in the isotypic Co-containing compound,[30] in contrast with the nonpuckered Ni layer in La_2INi_2.[14] The

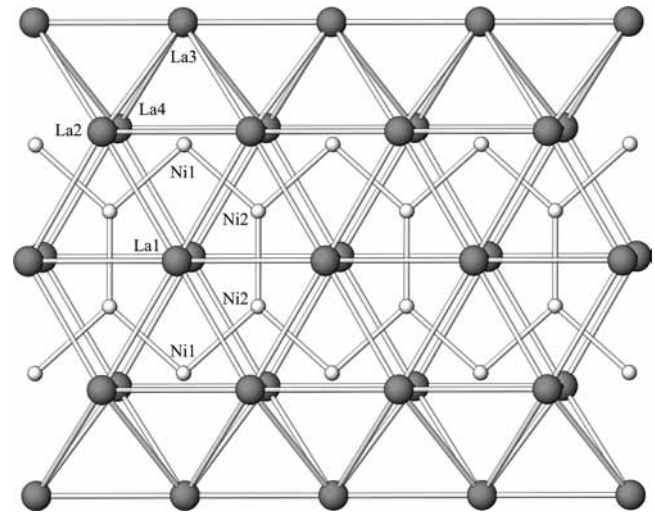

Figure 2. A La double trigonal prism chain with a Ni hexagon ribbon inside in the $La_8Br_7Ni_4$ crystal structure. The gray spheres are La and white are Ni. For clarity, Br atoms are not shown.

Scheme 1

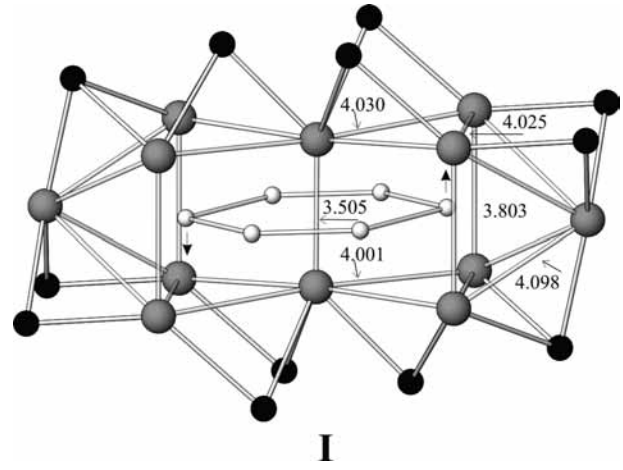

I

origin of this difference lies in the fact that, in the Gd_2IFe_2-type structure, only one trigonal face of the prism is capped by an I atom in an alternating way, whereas in the La_2INi_2 structure, both top and bottom triangular faces are either capped or free of I atoms, thus providing a charge-balanced neighborhood to the Ni atoms. It has been shown that the degree of puckering as well as the transition from the Gd_2IFe_2- to the La_2INi_2-type arrangement is determined in a distinct way by the relative sizes of the RE, I, and transition metal atoms.[30] In the $La_8Br_7Ni_4$ structure, the trigonal faces of the La_6 prisms are capped as in the Gd_2IFe_2 structure. Yet, the nonplanarity of the Ni ribbon is marginal. All Ni atoms (Ni2) at the shared hexagon edges are in the same plane. The other Ni atoms (Ni1) are out of the plane with a dihedral angle of 1.1° between the Ni2 plane and the Ni2−Ni1−Ni2 plane, resulting in a Ni1 to Ni2 plane distance of 0.03 Å. They shift away from the Br-capped triangular faces of the La_6 trigonal prism and La_5 square pyramid, as indicated by the two solid arrows in Scheme 1. Thus, on one corner of the Ni hexagon, Ni1 shifts downward, and on the other, upward (see Scheme 1), resulting in a "chair conformation" of the hexagon. At first sight, this conforma-

(23) Mattausch, Hj.; Oeckler, O.; Vajenine, G. V.; Kremer, R. K.; Simon, A. *Solid State Sci.* **1999**, *1*, 509.
(24) Mattausch, Hj.; Oeckler, O.; Simon, A. *Inorg. Chim. Acta* **1999**, *289*, 174.
(25) Mattausch, Hj.; Oeckler, O.; Zheng, C.; Simon, A. *Z. Anorg. Allg. Chem.* **2001**, *627*, 1523.
(26) Ruck, M. *Z. Anorg. Allg. Chem.* **1997**, *623*, 243.
(27) Wahl, B. U.; Doert, T.; Söhnel, T.; Ruck, M. *Z. Anorg. Allg. Chem.* **2005**, *631*, 457.
(28) Minyaev, R. M.; Hoffmann, R. *Chem. Mater.* **1991**, *3*, 547.
(29) Ruck, M.; Simon, A. *Z. Anorg. Allg. Chem.* **1993**, *619*, 327.
(30) Lefevre, C.; Hoch, C.; Kremer, R. K.; Simon, A. *Solid State Sci.* **2008**, in press.
(31) Babizhetskyy, V.; Zheng, C.; Mattausch, Hj.; Simon, A. *J. Solid State Chem.* **2007**, *180*, 3515.
(32) Saillard, J.-Y.; Hoffmann, R. *J. Am. Chem. Soc.* **1984**, *106*, 2006.
(33) Sheldrick, G. M. *SADABS*, version 2006/1; University of Göttingen: Göttingen, Germany, 2006.

Scheme 2

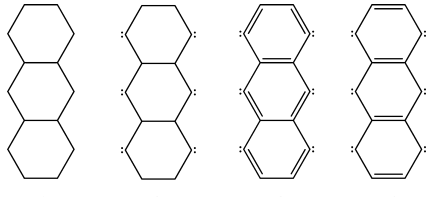

II

tion appeared to be of electronic origin. However, with a closer examination of the Ni coordination environment, the bending of the ribbon should be attributed to the packing of anions around Ni. As a result of the Br capping of the triangular faces of the La_6 cages, the normal to the Ni2 plane is also tilted relative to the vertical La1−La1 edge of the La_6 trigonal prism by 2.6°. The only small deviation from the planarity of the Ni ribbon corroborates the arguments put forward in ref 30.

With the anionic Ni centering the cationic La cages, the different La−La distances can also be rationalized. In the double La prisms shown in Scheme 1, the shortest La−La distance (3.505 Å) is at the center of the double prisms because these two La cations feel most anionic Ni attractions. The next shortest La−La distance (3.803 Å) is at the rectangular faces of the La_6 prism where the attraction is weaker. The distances at the triangular faces of the La_6 prism and La_5 pyramid are the longest because these faces are capped by Br atoms, which cannot get too close to each other due to their anionic charges.

Electronic Structure. A formal electron partition of $(La^{3+})_8(Br^-)_7Ni_4 \cdot 17e^-$ assuming Ni in a d^{10} configuration shows that there are 17 framework electrons per formula, which can be used for La−La, La−Ni, and Ni−Ni bonding. When some of the electrons are assigned to Ni, the electronic structure of $La_8Br_7Ni_4$ can be made analogous to that of a reduced rare earth metal halide with a main group endohedral. There are several ways to make the assignment. The first (see Scheme 2), $(La^{3+})_8(Br^-)_7(Ni^{3-})_2(Ni^{2-})_2 \cdot 7e^-$, with the inner Ni^{3-} isoelectronic to B and the outer Ni^{2-} to Be, would make all Ni−Ni contacts single bond. The second (**2**), $(La^{3+})_8(Br^-)_7(Ni^{3-})_2(Ni^{4-})_2 \cdot 3e^-$, is similar to the first except for an extra lone pair on the outer Ni. The third (**3**), $(La^{3+})_8$

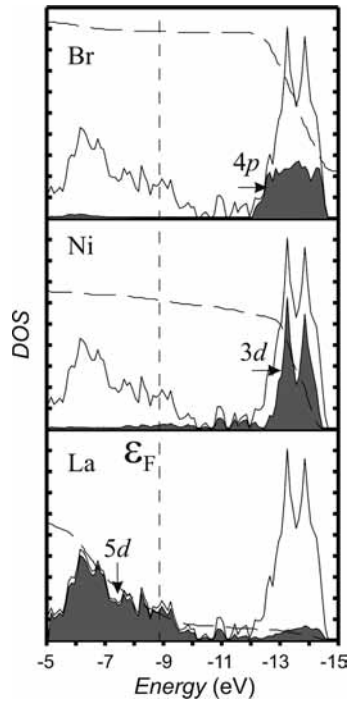

Figure 3. Calculated EH DOS for $La_8Br_7Ni_4$. The solid curves represent the total DOS; the shaded areas and dashed curves correspond to the contribution from the particular atom kind indicated in the panel and its integrated value, respectively. The vertical dotted line indicates the Fermi level.

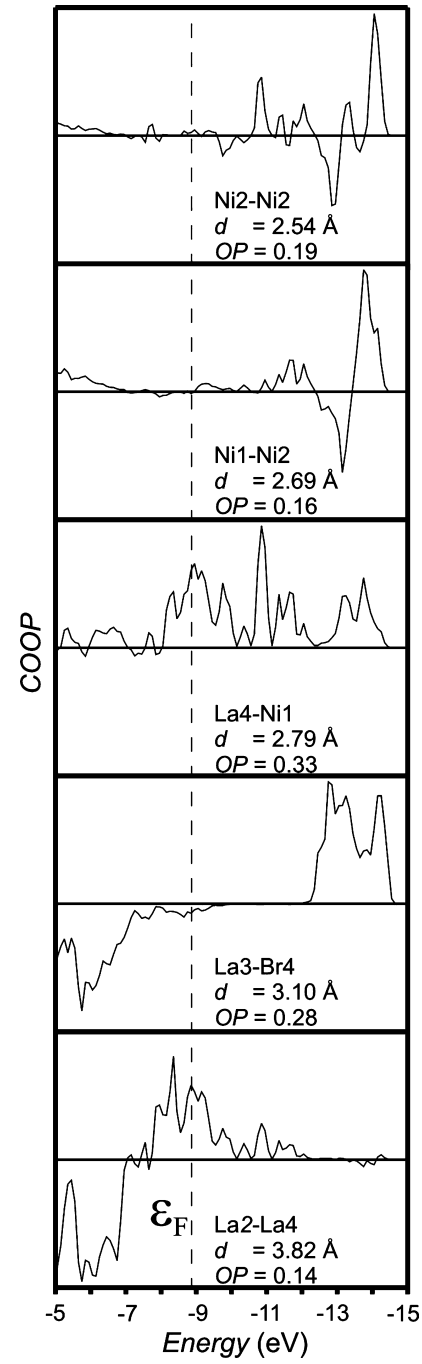

Figure 4. EH COOP curves of representative bonds in $La_8Br_7Ni_4$. The + region is the bonding area and the − region the antibonding area. The bond type, distance, and integrated overlap population up to the Fermi level are indicated in each panel. The vertical dotted line represents the Fermi level.

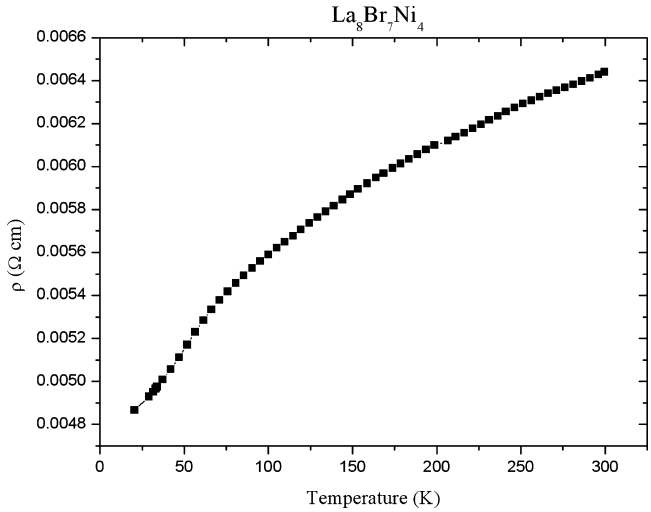

Figure 5. Resistivity as a function of temperature for a powder crystalline $La_8Br_7Ni_4$ sample.

$(Br^-)_7(Ni^{4-})_2(Ni^{5-})_2 \cdot h^+$, corresponding to a polyacene-like Ni ribbon, however, is unrealistic, as it requires more electrons than available. The fourth (**4**), $(La^{3+})_8(Br^-)_7(Ni^{4-})_4 \cdot e^-$ is quinoidic. This assignment is the most reasonable one considering the inner Ni−Ni bond is much shorter (2.529 Å) than the outer one (2.692 Å). The Ni−Ni distances are rather comparable to the Al−Al distances in the topologically similar Al hexagon ribbons in the $La_3I_2Al_2$ structure (2.550 and 2.615 Å). At first sight, however, the larger average Ni−Ni distance compared to that of Al−Al is a surprise, as the metallic radius of Al, 1.432 Å, is larger than that of Ni, 1.246 Å. The larger Ni−Ni distance is most probably due to the higher charges of anionic Ni, and the nearly identical inner Al−Al and Ni−Ni distances justify the assumption of a quinoidic character of the Ni hexagon. The calculated EH charges for the two types of Ni atoms (inner and outer positions in the ribbon) differ only by 0.1 e^-, in agreement with the equal charge assignment for the quinoidic species. This type of assignment has also been applied to the boron ribbon in Dy_2B_4C.[31]

Figures 3 and 4 show the EH DOS and COOP calculated for the experimental crystal structure of $La_8Br_7Ni_4$, respectively. For clarity, the energy window does not include the low-lying Br 4s state. The filled Ni 3d state is localized in the −14 eV region, while the 4s and 4p states spread out around the Fermi level. According to the EH calculation, about 1/3 of the s and p states are occupied, and they contribute to bonding. A significant amount of the La 5d state is below the Fermi level, indicating significant La−La interaction. In Figure 4, the top two panels show that there is the typical COOP feature for a filled d band,[32] bonding in the bottom half and antibonding at the top. Above the d band, the s and p states contribute mostly to bonding. The lower three panels demonstrate that all states below the Fermi level contribute to La−Ni, La−Br, and La−La bonding, as they typically do in a reduced rare earth metal halide. The EH calculations therefore indicate that the Ni−Ni bonding interaction is mostly contributed by the Ni 4s and 4p states, and the bonding pattern of $La_8Br_7Ni_4$ can be easily understood when Ni is treated as a charged species isoelectronic to the electronic configuration of a main group metal. Obviously, there is strong interaction between La and Ni, and a more realistic description should include the back-donation of charges from Ni to La, as indicated by the occupation of some La 5d state.

Physical Properties. The physical properties of $La_8Br_7Ni_4$ are in agreement with the analysis of the chemical bonding described above. The resistivity measured in the temperature range from 20 to 300 K is shown in Figure 5. It demonstrates a metallic behavior. The magnetic susceptibility measurement (not shown here) revealed a temperature-independent Pauli paramagnetism typical of a metal. There was a trace amount of Ni which contributed to the susceptibility, but with increasing magnetic field, a saturation occurred, clearly indicating the presence of the trace impurity.

Acknowledgment. We thank V. Duppel for assisting the EDX measurement, E. Brücher for the magnetic susceptibility measurements, G. Siegle for the conductivity measurements, and C. Kamella for help with the drawings.

Supporting Information Available: Listing of X-ray crystallographic details in the CIF format. This material is available free of charge via the Internet at http://pubs.acs.org.

IC801227E